IMMUNOLOGY

Targeting IL-1 controls refractory pityriasis rubra pilaris

Eloi Schmauch[1,2,3]†, Yannik Severin[4]†, Xianying Xing[5], Aaron Mangold[6], Curdin Conrad[7], Pål Johansen[8], J. Michelle Kahlenberg[5], Mark Mellett[8], Alexander Navarini[9], Stefan Nobbe[8,10], Mrinal K. Sarkar[5], Abhigyan Satyam[11], Lam C. Tsoi[5], Lars E. French[12,13], Jakob Nilsson[14], Suvi Linna-Kuosmanen[1,3], Minna U. Kaikkonen[3], Berend Snijder[4], Manolis Kellis[1,2], Johann E. Gudjonsson[5,15], George C. Tsokos[11], Emmanuel Contassot[9]†, Antonios G. A. Kolios[8,11,16]*

Pityriasis rubra pilaris (PRP) is a rare inflammatory skin disease with a poorly understood pathogenesis. Through a molecularly driven precision medicine approach and an extensive mechanistic pathway analysis in PRP skin samples, compared to psoriasis, atopic dermatitis, healed PRP, and healthy controls, we identified IL-1β as a key mediator, orchestrating an NF-κB–mediated IL-1β–CCL20 axis, including activation of CARD14 and NOD2. Treatment of three patients with the IL-1 antagonists anakinra and canakinumab resulted in rapid clinical improvement and reversal of the PRP-associated molecular signature with a 50% improvement in skin lesions after 2 to 3 weeks. This transcriptional signature was consistent with in vitro stimulation of keratinocytes with IL-1β. With the central role of IL-1β underscoring its potential as a therapeutic target, our findings propose a redefinition of PRP as an autoinflammatory keratinization disorder. Further clinical trials are needed to validate the efficacy of IL-1β antagonists in PRP.

INTRODUCTION

Pityriasis rubra pilaris (PRP) is a rare and severe inflammatory skin disease with a poorly understood pathogenesis. Skin involvement is characterized by an erythrodermic phase with long-term impairment of skin health that can involve the entire body surface. Several clinical types have been phenotypically defined, with the most common being the classical adult type (type I) (*1*). It presents with unique features including salmon-colored erythema, waxy palmoplantar keratoderma, and follicular centric papules as well as traits of psoriasis and atopic dermatitis (AD).

Although there is some evidence to suggest that the interleukin-23 (IL-23)/T helper 17 (T_H17) axis might play a role in PRP, the specific molecular mechanisms driving its pathogenesis are not well-defined (*2*). This lack of understanding is reflected in the variable responses to treatments. Current approaches include topical and systemic prednisone, non-biologic disease modifying antirheumatic drugs (DMARDs) such as methotrexate and retinoids, as well as biologicals targeting tumor necrosis factor (TNF), IL-23, and IL-17, which have shown only partial efficacy. For example, response rates of 75% psoriasis area and severity index (PASI75) improvement have been reported after 24 to 28 weeks in 50% of patients treated with IL-17 inhibitors (*3*, *4*). Phototherapy may actually worsen PRP symptoms in some cases (*5*). The variable and partial response rates in therapies of PRP highlight our limited understanding of the disease and the need for more effective therapeutic strategies.

We endeavored to unveil the mechanisms underlying PRP through a molecularly driven precision medicine approach. Our investigation involved a comprehensive molecular characterization of a monocentric PRP cohort, and, through extensive mechanistic pathway analysis, we identified IL-1β as a pivotal upstream regulator. To validate our findings clinically, we treated three patients who had previously failed targeted biological treatments with IL-1 antagonists. All three exhibited rapid and substantial clinical improvement upon receiving the IL-1 receptor antagonist (IL-1Ra) anakinra or the IL-1β inhibitor canakinumab. This robustly confirms the distinctive role of IL-1β in the pathogenesis of adult-type PRP.

RESULTS

The PRP skin transcriptome differs from other IMIDs

To elucidate the molecular signature of PRP, we examined three transcriptomic cohorts (Fig. 1A). We examined Cohort A to differentiate PRP from other related immune-mediated inflammatory diseases (IMIDs), and it consisted of a targeted transcriptomic assessment of lesional skin from patients with adult-type PRP (18 active and 8 post-PRP samples), six psoriasis, seven AD, and eight healthy control (HC) samples (Fig. 1, A and B). Detailed demographic, clinical, and treatment information for cohort A is presented for comparison (table S1). In brief, we took 12 of the 18 PRP, two of the six psoriasis, and six of the seven AD samples from participants with moderate or more severe disease. Analysis of differentially expressed genes (DEGs) in PRP versus the other conditions revealed a distinct inflammatory pattern associated with PRP (Fig. 1C and fig. S1 and S2)

[1]Broad Institute of MIT and Harvard, Cambridge, MA 02142, USA. [2]Computer Science and Artificial Intelligence Laboratory, Massachusetts Institute of Technology, Cambridge, MA 02139, USA. [3]A.I. Virtanen Institute for Molecular Sciences, University of Eastern Finland, Kuopio, Finland. [4]Institute of Molecular Systems Biology, Department of Biology, ETH Zurich, 8049 Zurich, Switzerland. [5]Departments of Internal Medicine and Dermatology, University of Michigan, Ann Arbor, MI 48109, USA. [6]Department of Dermatology, Mayo Clinic Arizona, Scottsdale, AZ 85259, USA. [7]Department of Dermatology, CHUV University Hospital and University of Lausanne (UNIL), Lausanne, Switzerland. [8]Department of Dermatology, University of Zurich and University Hospital Zurich, Zurich, Switzerland. [9]Department of Biomedicine and Dermatology Department, University Hospital of Basel, Basel, Switzerland. [10]Department of Dermatology, Cantonal Hospital Frauenfeld, Frauenfeld, Switzerland. [11]Department of Medicine, Beth Israel Deaconess Medical Center, Harvard Medical School, Boston, MA 02215, USA. [12]Department of Dermatology and Allergology, Ludwig Maximilian University of Munich, Munich, Germany. [13]Dr. Philip Frost, Department of Dermatology and Cutaneous Surgery, University of Miami Miller School of Medicine, Miami, FL 33125, USA. [14]Department of Immunology, University Hospital Zurich, Zurich, Switzerland. [15]Taubman Medical Research Institute, University of Michigan, Ann Arbor, MI 48109, USA. [16]University of Zurich, Zurich, Switzerland.
*Corresponding author. Email: akolios@bidmc.harvard.edu
†These authors contributed equally to this work.

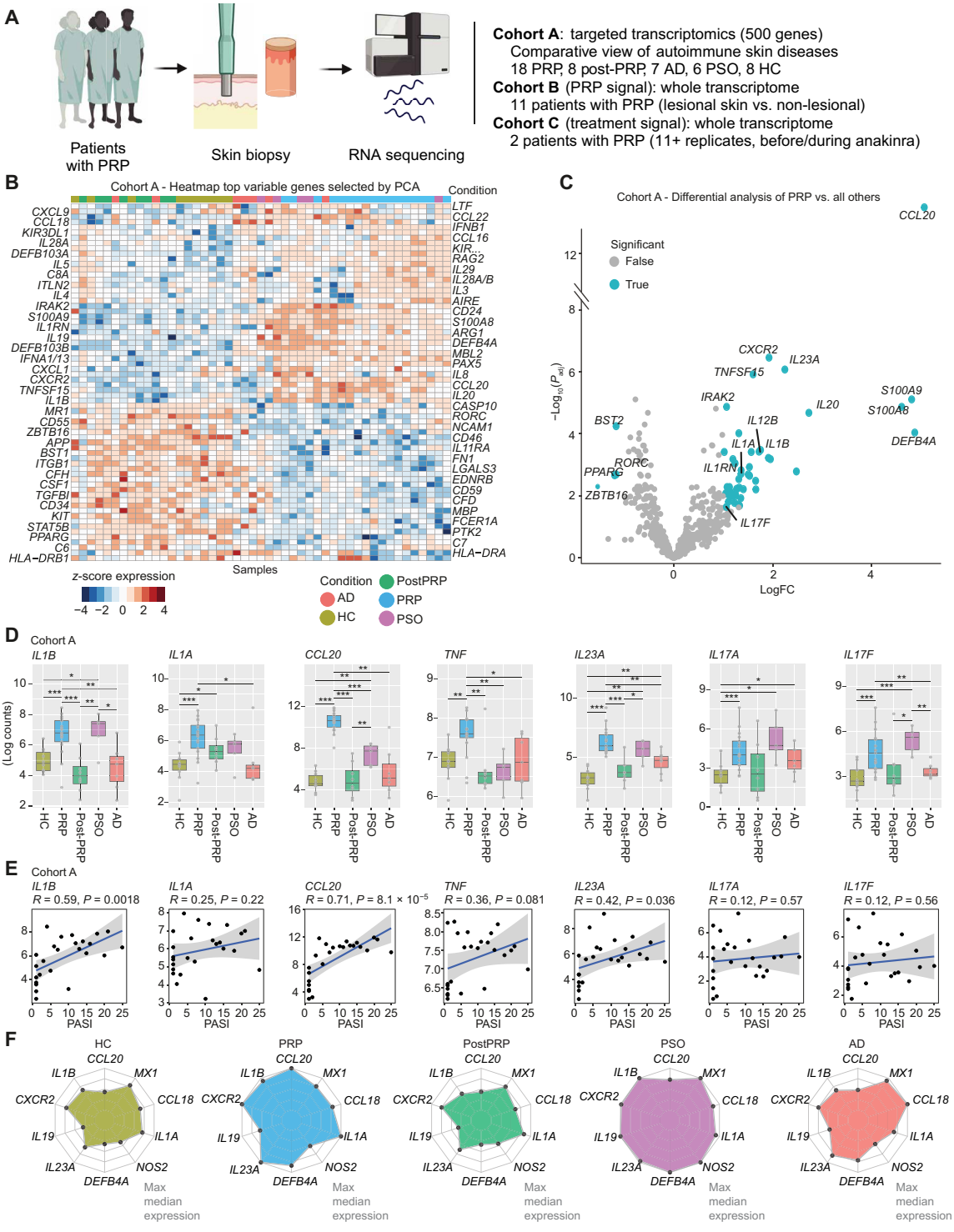

Fig. 1. Comparative transcriptomic analysis across PRP versus other cutaneous inflammatory diseases. (**A**) Study overview. This study uses three transcriptomic cohorts to elucidate the molecular mechanisms of PRP. Cohort A explores the transcriptomic landscape of PRP, alongside that of other cutaneous inflammatory diseases (psoriasis and atopic dermatitis), patients after PRP (post-PRP), and healthy controls (HCs). Cohort B explores PRP signature at the whole transcriptome level, while cohort C explores the treatment response signature. Created with Biorender.com. (**B**) Heatmap displaying the top differentially expressed genes (DEGs) in cohort A as determined by principal components analysis (PCA). (**C**) Differential gene expression analysis comparing PRP samples to all other samples in cohort A. Colored points indicate significantly DEGs ($P_{adj} < 0.05$) with a log fold change greater than 1. (**D**) Boxplots demonstrating the expression (log_{10} counts) of selected genes across different disease types (cohort A). (**E**) Scatter plot correlating selected gene expression in PRP and post-PRP samples with corresponding PASI scores (cohort A). PRP ($n = 13$), post-PRP ($n = 8$), psoriasis (PSO; $n = 6$), AD ($n = 7$), and HC ($n = 8$). (**F**) Spider plots representing selected genes across different diseases. The median expression for each group was calculated and normalized to the maximum values per gene.

with significantly increased expression of genes encoding cytokines for *IL1A*, *IL1B*, *IL23A*, *IL17A/F*, *TNF*, chemokines *CCL18* and *CCL20*, and defensin/alarmins *S100A8/9* and *DEFB4A* (Fig. 1D). The transcriptional signature characteristic for PRP included *IL1B* and *CCL20* as the predominant DEGs, whose expression significantly correlated with clinical severity of PRP measured by PASI ($P = 0.0018$ and < 0.0001 for *IL1B* and *CCL20*, respectively), indicating a pathogenic relevance (Fig. 1E). The identification of Chemokine (C-C motif) ligand 20 (CCL20) and its association with clinical severity was already previously reported (*6*–*8*). In summary, PRP embodies a unique transcriptional profile compared with related IMIDs (Fig. 1F), thereby suggesting a distinct pathophysiology and an involvement of IL-1β and CCL20.

IL-1β is a key regulator of PRP and linked to keratinization

To confirm our findings more broadly, we constructed a regulatory network of PRP to further dissect its molecular signature. We analyzed publicly available data of patients with PRP with paired lesional versus non-lesional skin biopsies [constituting cohort B (*4*), Fig. 1A]. Ingenuity pathway analysis (IPA) identified *IL1B* as the second strongest predicted upstream regulator of the PRP transcriptomic signature in that cohort (Fig. 2A). A subsequent gene-gene co-expression analysis identified 10 co-expressed gene clusters (Fig. 2B and fig. S3A) where *IL1B*-containing cluster 1 notably overlapped with the PRP signature and demonstrated the highest percentage of significant PRP-DEGs among all clusters (Fig. 2C). Furthermore, cluster 1 genes exhibited a notable log-fold increase in all genes that

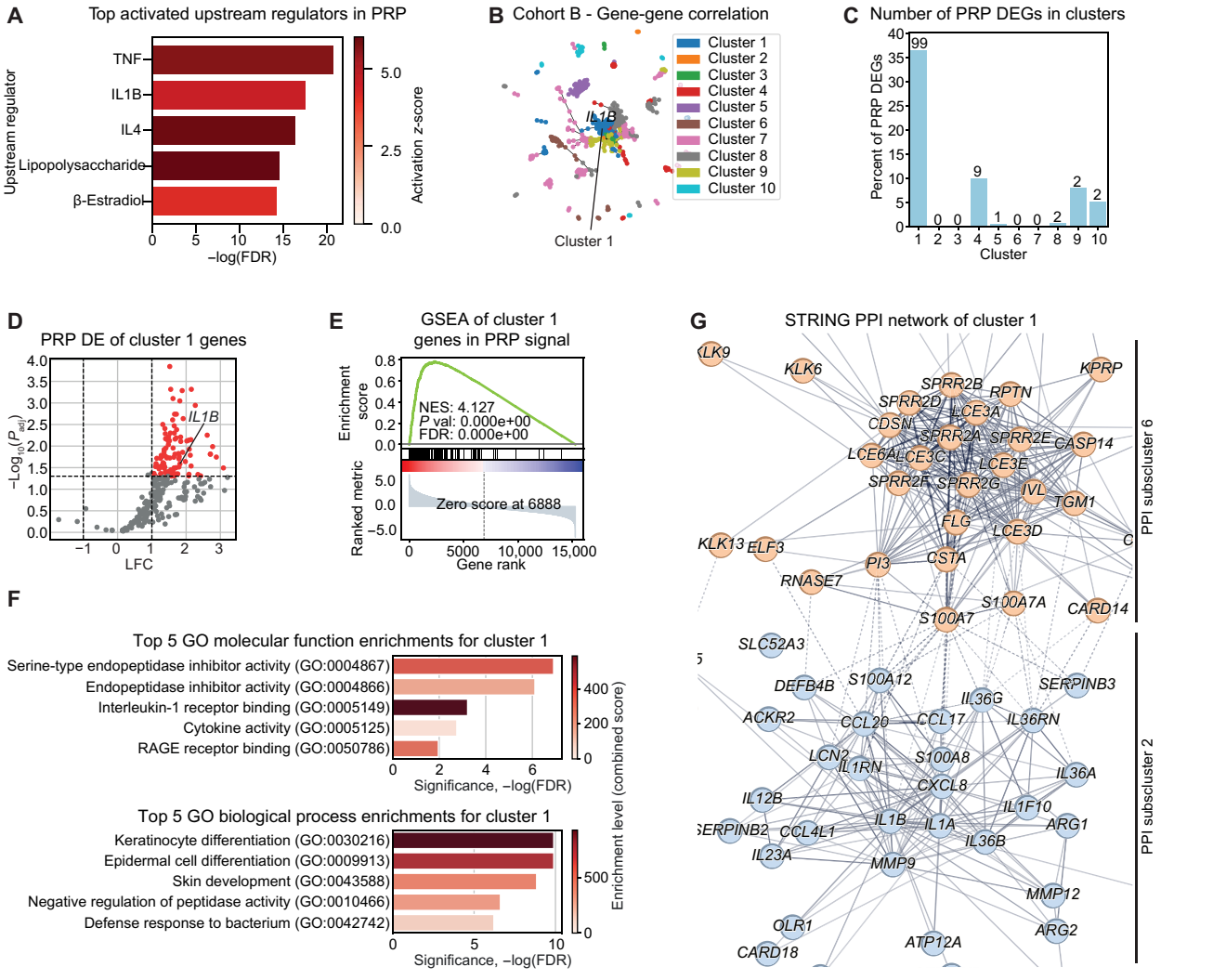

Fig. 2. Deep analysis of PRP biopsy RNA-seq data identifying a PRP molecular network with a central role of IL-1 signaling and IL-1β. (**A**) Top five activated IPA upstream regulators from paired PRP versus control differential expression (DE) analysis, in untreated patients (cohort B). (**B**) Correlation analysis network from cohort B. Genes are colored by clusters. Cluster 1 contains *IL1B*. (**C**) Distribution of PRP DEGs across the 10 correlation clusters. The numbers on the bars are the numbers of genes in each cluster having significant DE in PRP ($P_{adj} < 0.05$). The scale of the *y* axis is the percentage of genes in that cluster that had significant DE in PRP ($P_{adj} < 0.05$). (**D**) Volcano plot of PRP DE results of genes belonging to the correlation cluster 1. Red: logFC >1, $P_{adj} < 0.05$. (**E**) GSEA of PRP versus control DE for correlation cluster 1 (gene set, module 1 genes; DE, PRP signal; cohort B). NES, normalized enrichment score. (**F**) Correlation cluster 1 overrepresentation analysis (ORA; gene set enrichment), in GO molecular function (top plot), and GO biological process (bottom plot). GO, gene ontology. (**G**) STRING protein-protein interaction (PPI) network analysis for the correlation cluster 1 genes, with zoom-in to the two main PPI subclusters. Zoomed-out image is in fig. S3F.

were shared with PRP-DEGs (Fig. 2D), and their enrichment/predominance in PRP was confirmed by gene set enrichment analysis (GSEA) (Fig. 2E).

Gene set overrepresentation analysis (ORA) of the cluster 1 exposed connections with immune and inflammatory signals, including IL-1 receptor binding, and with keratinocyte differentiation (Fig. 2F and fig. S3B). We subsequently dissected cluster 1 into eight functional subclusters (Fig. 2G and figs. S3C and S4A) using Search Tool for the Retrieval of Interacting Genes/Proteins (STRING) functional network analysis [protein-protein interaction (PPI)]. The two primary subclusters relate to keratinization (orange) and IL-1/inflammation (blue, Fig. 2G). The IL-1/inflammation subcluster included eight genes from the IL-1 family: *IL1A*, *IL1B*, *IL36A*, *IL36G*, *IL36RN*, *IL1RN*, *IL1F10*, and *IL36B*, as well as *CCL20*, *IL23A*, *CARD14*, and *S100A8*. Both subclusters exhibited strong interaction with each other. Enrichment of each cluster confirmed these annotations (ORA; fig. S4, B and C), which contained a substantial number of genes overexpressed in PRP (fig. S4, D and E). This analysis provides strong evidence that the immune pathways involving IL-1 are closely intertwined with keratinization mechanisms in PRP. In summary, these findings advocate targeting of IL-1 for the management of PRP.

Treatment of PRP with IL-1 antagonists rapidly ameliorates disease

To validate the potential of IL-1β blockade for PRP treatment, we treated three patients with therapy-refractory PRP (two males, ages 53 and 59, and one female, age 53) with the IL-1Ra anakinra (Fig. 3, A and B, and fig. S5, A to D). We describe patient characteristics and previous therapies in table S2. Disease duration until the start of treatment of patients 1 to 3 was 36, 9, and 7 months, respectively.

Patient 1 initially responded well to a standard anakinra dose of 100 mg/day with 50% improvement in psoriasis skin severity index (PASI50) at week 2 (Fig. 3, C and D). At week 6, the disease worsened, and the anakinra dosage was doubled to 200 mg/day. Patients 2 and 3 also received the same dose regimen resulting in a PASI50 at week 2 for patient 2 and at week 3 for patient 3 (Fig. 3, E and F). PASI75 was reached by week 8 in patients 1 (PASI of 11.4 to 2.6, ΔPASI of 77%) and 2 (PASI of 21.4 to 5.7, ΔPASI of 73%) and by week 12 in patient 3 (PASI of 34.2 to 9.4, ΔPASI of 73%). After week 12, patients 1 and 2 stopped treatment due to lack of health insurance cost coverage. Patient 2 continued to improve and reached complete resolution without any other treatment. Patient 1 was subsequently switched to biologics targeting TNF, IL-23, or IL-17, none of which adequately controlled the disease (Fig. 3D and table S2). When switched to the anti–IL-1β monoclonal antibody canakinumab, patient 1 improved within 8 weeks (ΔPASI of 85%) (Fig. 3D and fig. S5E). Patient 3 developed treatment-related eosinophilia, which required dose reduction of anakinra to 100 mg/day. Eosinophilia improved but PRP worsened (PASI of 17.1, ΔPASI of 49%); therefore, patient 3 was switched to canakinumab as well. This resulted in further PASI improvement within 5 weeks (PASI of 5.7, ΔPASI of 83%; Fig. 3F and fig. S5E) in the absence of eosinophilia. Apart from this case of transient eosinophilia, all patients tolerated the treatment well and were able to reduce topical steroid use.

We histologically confirmed the clinical improvement in all patients (Fig. 3, G to K, and fig. S5F), which included normalization of IL-1β expression at week 8, reaching similar levels to those in non-lesional tissue (Fig. 3H and fig. S5F). In addition, we found reduction of *CCL20* expression during treatment and the presence of caspase-1 (CASP-1) at baseline (fig. S5, G and H). Also, itch, on a numeric rating scale (NRS) from baseline to week 8, reduced from 10/10 to 1/10 in patient 1 (90%) and from 5/10 to 0/10 (100%) in patient 2. Patient 3 did not have symptoms like itch (stable NRS of 2/10 during treatment). We did not find any mutations in *CARD14* in any of the three patients (fig. S6).

Dermatology Life Quality Index (DLQI) from baseline to week 12 reduced from 26 to 2 (92%) in patient 2, 27 to 24 (11%) in patient 1 and remained stable at 17 in patient 3. During follow-up, while patient 1 was on different biological therapies but not responding sufficiently, DLQI remained between 18 and 24. Twelve weeks after switching to canakinumab, the DLQI dropped to 8. Also in patient 3, 5 weeks after starting and responding to canakinumab, DLQI dropped to 8.

Patient 2 showed nail involvement (pitting and distal onycholysis, all fingernails), which, from week 6 on, improved until complete remission at week 12. Patient 1 reported arthralgias in elbow, shoulder, and hips, initially NRS of 7/10, which almost vanished during anti–IL-1 treatments. All patients reported photosensitivity and PRP worsened upon ultraviolet (UV) B phototherapy in patients 1 and 2. Together, we report a rapid and successful response to the IL-1 antagonists anakinra and canakinumab in all three patients with PRP, underscoring the importance of IL-1β in PRP disease pathogenesis.

Adverse events do not show any previously unknown safety signals

While patient 2 did not report any adverse events, patient 1 reported a mild tiredness in the first 3 days of anakinra treatment and a slightly painful injection site reaction (swelling) between weeks 2 and 6, which resolved almost completely afterward. Patient 3 showed neglectable injection site reactions during anakinra treatment. In addition, after the first 12 weeks of anakinra, an eosinophilia occurred, which peaked at week 15 with 3.1 g/liter. After exclusion of differential diagnosis, this was interpreted as treatment related to anakinra. Anakinra was reduced to 100 mg daily, and eosinophilia improved (0.7 g/liter), but PRP worsened subsequently (PASI of 17.1). The patient switched to canakinumab, with decreasing PRP symptoms (PASI of 5.7 at week 5 after canakinumab initiation) and with absence of eosinophilia.

Anakinra reverses the PRP transcriptional signature in patients with PRP

We sought to dissect the mechanisms involved in the development of PRP by exploring the transcriptional signature following treatment (cohort C, Fig. 1A) and to confirm IL-1β as a potential target. All top five positive upstream regulators in active PRP (cohort B (*4*), Fig. 2A) showed significant down-regulation upon treatment targeting IL-1β in our patients (Fig. 4A).

Positive DEGs in active PRP before treatment exhibited significant negative enrichment in the treatment signal (Fig. 4B). Furthermore, GSEA of selected pathways of interest, such as TNF-α signaling via nuclear factor κB (NF-κB), showed positive enrichment with PRP and negative enrichment following IL-1 antagonist treatment (Fig. 4C). Overall, predicted activation scores of IPA annotations for disease, pathways, and upstream regulators displayed a significant negative correlation between PRP [in cohort B (*4*)] and the treatment signal (Fig. 4D). We define the treatment signal as the

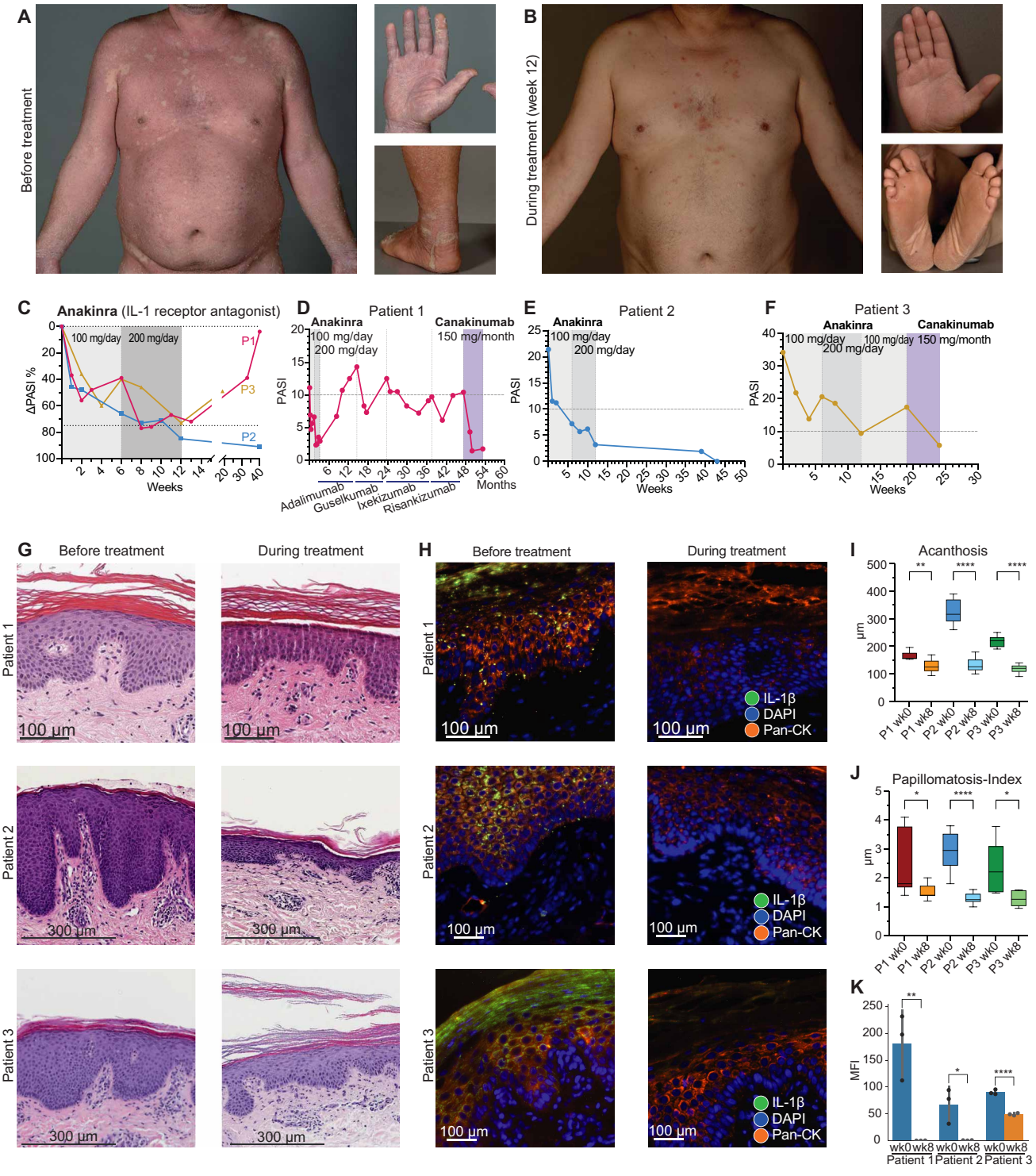

Fig. 3. Clinical course of patients during anti–IL-1 treatment. (**A** and **B**) Patient 1 before (A, week 0) and during (B, week 12) anakinra treatment. (**C**) ΔPASI improvement (%) during anakinra treatment in patients 1 to 3. Dose of 100 mg/day from weeks 0 to 6 and of 200 mg/days from weeks 6 to 12. P1, patient 1; P2, patient 2; P3, patient 3. (**D** to **F**) Treatment course of all three patients, with respective PASI score. The time course started at the beginning of anakinra treatment. Anakinra, 100 or 200 mg/day (gray shade). Canakinumab, 150 mg/month (purple). Patient 1 was treated with many biologics, but only anakinra and canakinumab proved effective (D). Patient 2 was successfully treated with anakinra (E). Patient 3 saw a positive response under both anakinra and canakinumab (F). (**G**) Representative hematoxylin and eosin staining from weeks 0 and 8 in patients 1 to 3. (**H**) Representative IL-1β immunofluorescence stainings from weeks 0 and 8 in patients 1 to 3. Scale bars, 100 µm. DAPI, 4′,6-diamidino-2-phenylindole. (**I**) Changes in acanthosis in all patients during treatment from weeks (wk) 0 and 8 (*$P \leq 0.05$, **$P \leq 0.01$, and ****$P \leq 0.0001$). (**J**) Changes in papillomatosis index in all patients during treatment from weeks 0 and 8. (**K**) Mean fluorescence intensity (MFI) of IL-1β expression from the three patients, in lesional skin before and after treatment. *$P \leq 0.05$, **$P \leq 0.01$, and ****$P \leq 0.0001$.

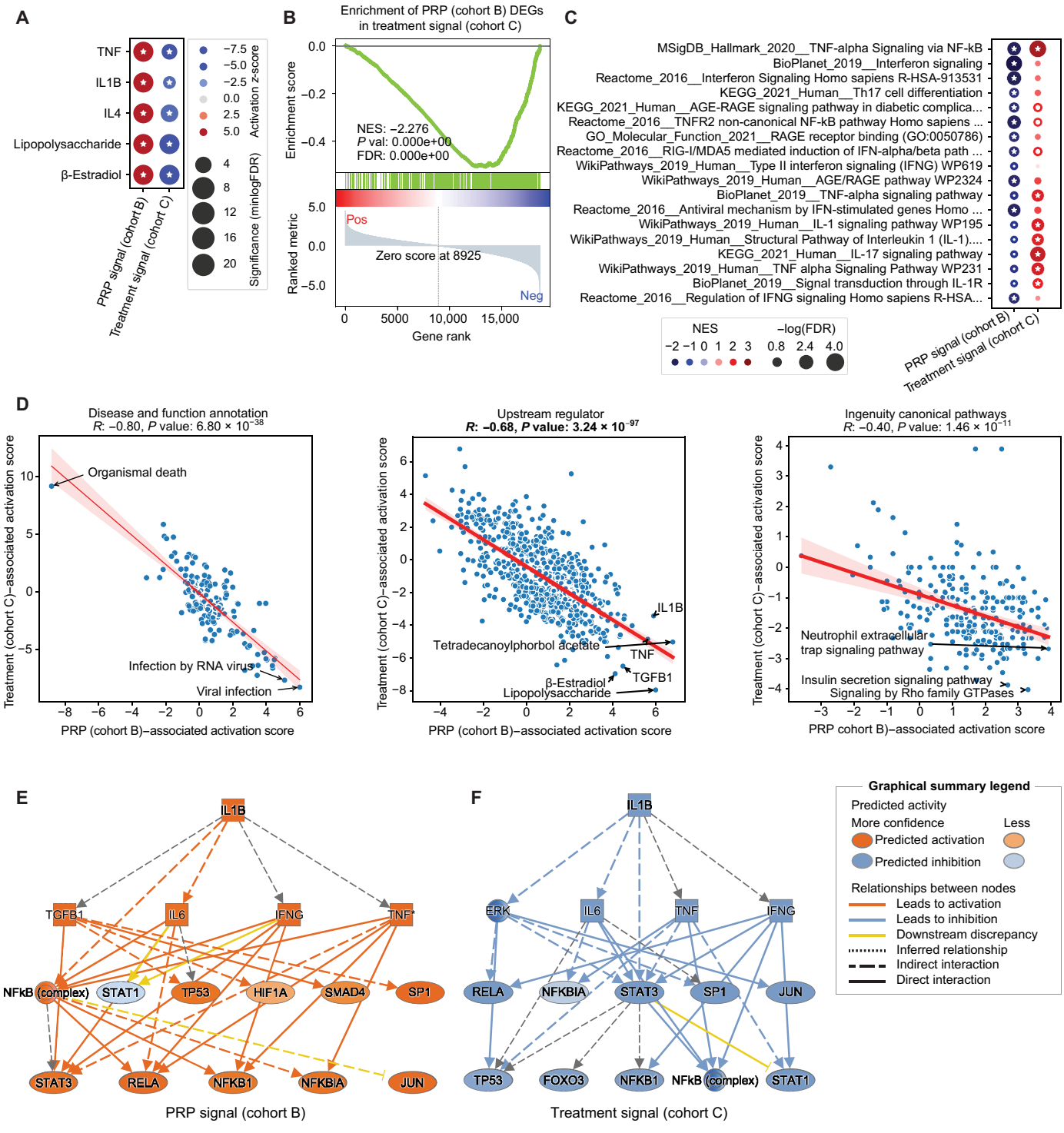

Fig. 4. Anti–IL-1β treatment–associated PRP transcriptional signature reversion. (**A**) Comparison of top PRP-associated IPA upstream regulators in PRP signal (cohort B) and treatment signal (cohort C). (**B**) GSEA with significant DEGs from PRP signal (cohort B) and treatment signal (cohort C) DE analysis. Pos, positive; Neg, negative. Here, PRP signal–associated genes with FDR < 0.05 and LFC > 0 constitute the gene set on which GSEA is run. (**C**) GSEA results of pathways of interest in PRP signal (cohort B) and treatment signal (cohort C). (**D**) Comparison of activation score of IPA enrichment (left to right: disease/function annotations, upstream regulators, and IPA canonical pathways), which are predicted to be associated with both PRP signal (cohort B) and treatment signal (cohort C). GTPases, guanosine triphosphatases. Pearson correlation and associated *P* values are calculated. (**E**) IPA upstream regulator mechanistic network of *IL1B* in PRP signal (cohort B). (**F**) IPA upstream regulator mechanistic network of *IL1B* in treatment signal (cohort C).

DEGs from analysis of lesional samples after versus before treatment in cohort C. IPA mechanistic network analysis further showed that gene regulation arising from *IL1B* could itself indirectly regulate *TNF*, *IFNG*, *IL6*, and *TGFB1*, with downstream activation of *NFkB* and *STAT1* (Fig. 4E), which reversed with treatment (Fig. 4F). The interaction of these cytokines is also supported by the IPA summary network of PRP [cohort B (*4*)] and treatment (cohort C) differential expression (DE) analysis, showing a central role of IL-1β (fig. S7). In summary, these results highlight a reversion of PRP transcriptional signals and NF-κB inhibition upon anakinra treatment.

IL-1β drives a PRP-specific transcriptomic signature in keratinocytes in vitro

Next, we assessed the impact of IL-1β signaling and activation in keratinocytes (Fig. 5A). DE analysis of IL-1β–stimulated keratinocytes revealed many shared DEGs with PRP signal (cohort B), associated with a significant correlation of their $\log_2$ fold change (LFC) (Fig. 5B and fig. S8A). This signal overlap is confirmed through GSEA (Fig. 5C). This experiment shows that IL-1β itself can up-regulate key element of the PRP molecular network that we previously describe, as we observe a significant up-regulation of genes encoding CCL20, IL-1β, TNF, IL-23A, IL-36γ, NF-κB1 (Fig. 5D and fig. S8B). In addition, IL-1β stimulation of keratinocytes leads to enrichments in pathways of inflammation, IL-1, and NF-κB, which also display enrichment in PRP (Fig. 5E and fig. S8, C to E). These in vitro keratinocyte data overlapping with the PRP molecular signature demonstrate the central role of IL-1β in keratinocytes for PRP pathogenesis and hint at the involvement of previously described downstream players such as CCL20, TNF, IL-23A, IL-36γ, Defensin Beta 4A (DEFB4A), IL-17C, C-X-C motif Chemokine Ligand 8 (CXCL8), and Nucleotide-binding oligomerization domain-containing protein 2 (NOD2) in inflammatory dermatoses.

The strongest up-regulated chemokine in the transcriptome analysis of lesional PRP skin (cohort A) was CCL20 (Fig. 1C). TNF and IL-1β were also the strongest inducers of CCL20 in keratinocytes in vitro (Fig. 5F and fig. S8F) and inhibition of IL-1 signaling with anakinra decreased CCL20 expression (fig. S5G), suggesting a major role of an IL-1β–CCL20 axis in disease pathogenesis.

NOD2 and CARD14 are the CARD proteins (caspase recruitment domain) with the strongest DE signal in PRP (cohort B, fig. S9A). Previous evidence strongly links CARD14 to PRP, and both genes are known to induce NF-κB (*9*). Both were significantly correlated with *IL1B*- and *NF-κB*–associated genes (fig. S9, B and C). NOD2 was also significantly up-regulated in active lesional versus active non-lesional or post-PRP (cohort A, CARD14 was not part of this targeted sequencing panel) (fig. S9D) and after IL-1β stimulation in keratinocytes in vitro (Fig. 5D). IPA prediction of the mechanistic network in the *PRP signal* (cohort B) confirms the downstream activation of NF-κB as being downstream of CARD14 and NOD2. That is also the case for BCL10, which is known to be activated by CARD14 and NOD2 (fig. S9C). Deep analysis of a *CARD14* gain-of-function (GOF) dataset in mice (*10*) revealed a similar molecular signature in keratinocytes than that we establish for IL-1β stimulation, including increased expression of *Nod2*, *Tnf*, *Irak2*, and *Il1b* itself (fig. S10A). In addition, GSEA of keratinocytes in that dataset linked *CARD14* GOF with pathways described earlier such as IL-1 signaling pathway, keratinization, and TNF-α signaling via NF-κB (fig. S10, A and B). *CARD14* and *NOD2* gene expression in cohort B display a strong correlation with *IL1B* (fig. S9B), which underscores their role in keratinocyte interactions within PRP-affected skin.

Apoptosis-associated speck-like protein containing a CARD (ASC)-speck formation, an indicator of canonical inflammasome activation, was undetectable in patients 1 and 2 as well as in five additional patients with active PRP. Immunohistochemistry showed caspase-1 expression (cohort C, fig. S5H); however, expression levels did not change between active versus post-PRP or lesional and non-lesional skin (cohort A, fig. S9D). Therefore, our findings suggest that IL-1β can be processed by caspase-1 in an ASC-independent manner.

Ultimately, the overlap of the gene signature in active PRP with IL-1β–stimulated keratinocytes suggests a crucial role for keratinocytes in the cutaneous inflammation that characterizes PRP, with NF-κB being a key downstream signaling molecule involved. Our results allow us to propose a new molecular mechanism at the basis of PRP pathophysiology (Fig. 6).

DISCUSSION

Our findings unequivocally establish the IL-1 pathway and IL-1β as pivotal upstream regulators in PRP pathogenesis, providing an important proof of principle of a molecularly guided precision medicine approach in this rare, chronic, and severe inflammatory skin disease. Treatment with IL-1 antagonists as a proof of concept in three patients with therapy-refractory PRP resulted in profound clinical improvement and a reversal of the PRP transcriptional signature in skin biopsies. Our work not only enhances the understanding of the mechanisms underlying PRP pathogenesis but also highlights the central role of the IL-1β pathway driving the disease.

The rare subtype of inherited PRP harbors *CARD14* GOF mutations that activate NF-κB signaling, leading to up-regulation of genes such as *CCL20* and *IL1B* in the epidermis (*9*), which has been confirmed in cell lines (*11*) and mouse models (*10*, *12*). In addition, patients with PRP without *CARD14* mutations also show *CARD14* overexpression (*13*). This suggests that both inherited and sporadic PRP share similar mechanisms, where overactive and/or overexpressed CARD14 activates NF-κB, leading to the expression of pro-inflammatory genes such as *CCL20* and *IL1B*. Analysis of a *CARD14* GOF dataset in mice (*10*) revealed similar gene transcript enrichments and molecular patterns to those observed in our studies (fig. S10, A and B). These results underline the classification of PRP, be it inherited or sporadic, as an autoinflammatory keratinization disorder.

Although CCL20 was the most DEG with PRP (Fig. 1), our network integration analysis of PRP transcriptional signal highlights the IL-1 pathway as a major regulator, highlighting its potential as a target.

Moreover, we observed *NOD2* overexpression in active and lesional PRP, which has also been described in *CARD14* GOF mice (*14*) and correlates with *IL1B* expression. As NOD2 is a cytoplasmic pattern recognition receptor for bacterial peptidoglycan motifs and activates the NF-κB pathway (*15*), this supports the hypothesis that a microbial response contributes to PRP pathogenesis.

The balance between IL-1 and IL-1Ra is a key element of inflammation (*16*), and a large excess (100- to 1000-fold) of IL-1Ra is necessary to block IL-1 activity in vitro and in vivo (*17*). Pro-inflammatory stimuli and an IL-1β peak can subsequently increase the *IL1RN* gene expression (*16*) and IL-1Ra production (*18*, *19*). We

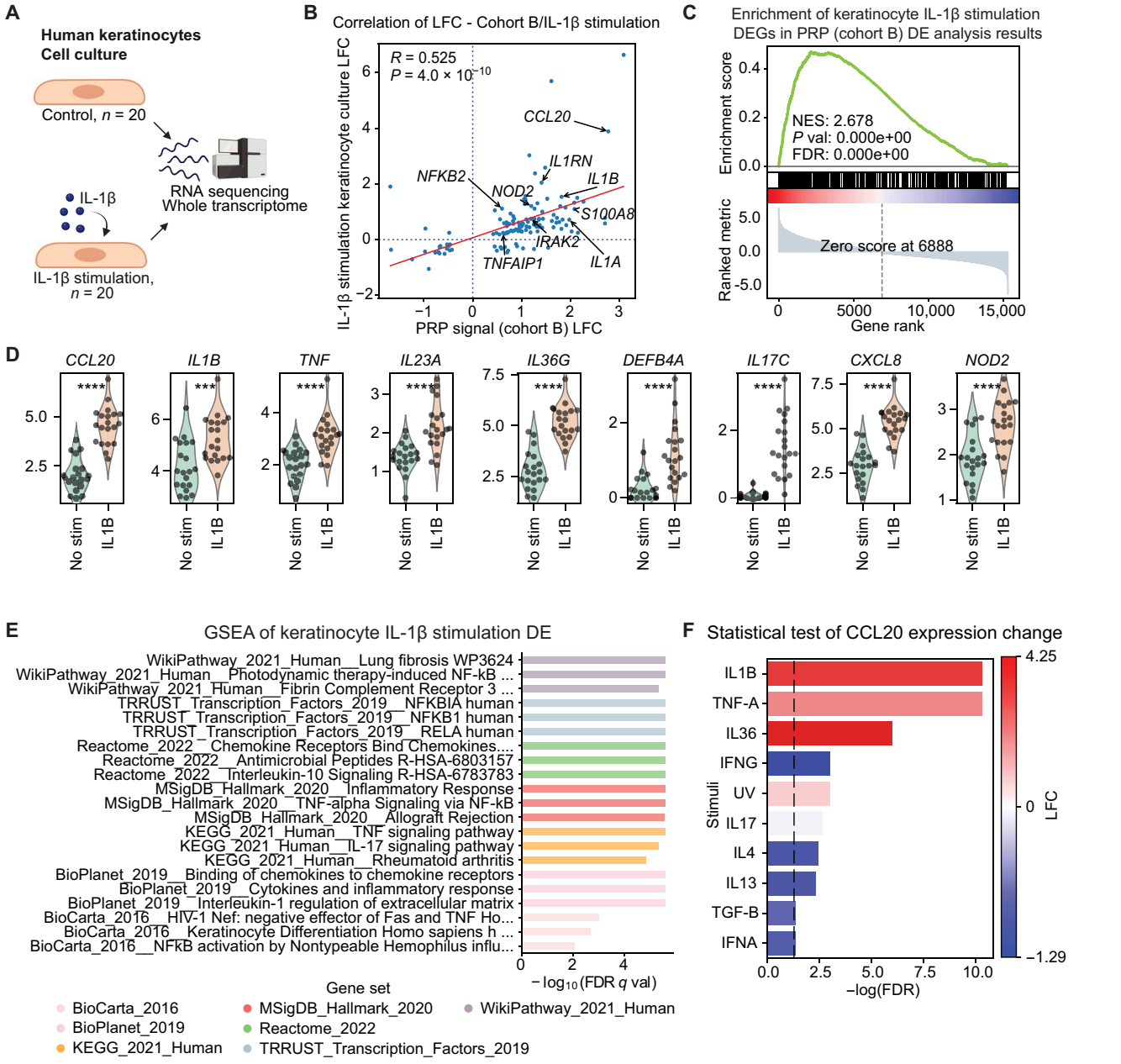

Fig. 5. IL-1β as a key element of the PRP pathogenesis mechanism. (**A**) Keratinocyte cultures derived from human samples were stimulated with IL-1β. RNA-seq was performed on 20 control and stimulated experiments, enabling the exploration of the transcriptomic response of human keratinocytes to IL-1β stimulation. Created with Biorender.com. (**B**) Correlation of logFC values for genes that are significantly DE ($P_{adj} < 0.05$) both in IL-1β stimulation and PRP (cohort B). Regression line is shown in red. The correlation was significant with $R = 0.525$ and $P = 4.0 \times 10^{-10}$. (**C**) GSEA results of positively DEGs with keratinocyte IL-1β stimulation (forming a gene set) on PRP (cohort B) DE results. (**D**) Expression distribution of *CCL20*, *IL1B*, *TNF*, *IL23A*, *IL36G*, *DEFB4A*, *IL17C*, *CXCL8*, and *NOD2* in keratinocyte cultures, with (IL1B) or without IL-1β stimulation (No stim). $^{*}P \leq 0.05$, $^{**}P < 0.01$, $^{***}P < 0.001$, and $^{****}P < 0.0001$. (**E**) Associated GSEA results of keratinocyte IL-1β stimulation DE. (**F**) Statistical test of CCL20 expression change. Significance of CCL20 expression differences across various stimuli compared to no stimulation using paired *t* test. The *x* axis displays the $-\log_{10}$(FDR) with a significance threshold at FDR = 0.05, represented by a dashed line. Color indicates stimulation associated with the expression log fold change (LFC). Bars surpassing the line are statistically significant.

show that *IL1RN* is significantly overexpressed after IL-1β stimulation of keratinocytes (fig. S8A) as well as present in our PRP network analysis with its two primary subclusters related to keratinization and IL-1/inflammation (Fig. 2G). We believe that this balance is in favor of IL-1β in PRP. Through treatment with anakinra, the recombinant version of IL-1Ra, or by blocking IL-1β with canakinumab, we aimed to rebalance the equilibrium toward the healthy state.

Our clinical and molecular data also underline that IL-1β signaling is necessary for sustained NF-κB activation in PRP, as confirmed with in vitro IL-1β–stimulated keratinocytes. Of note, CCL20 acts as a mediator of inflammation and a chemoattractant (via the CCR6

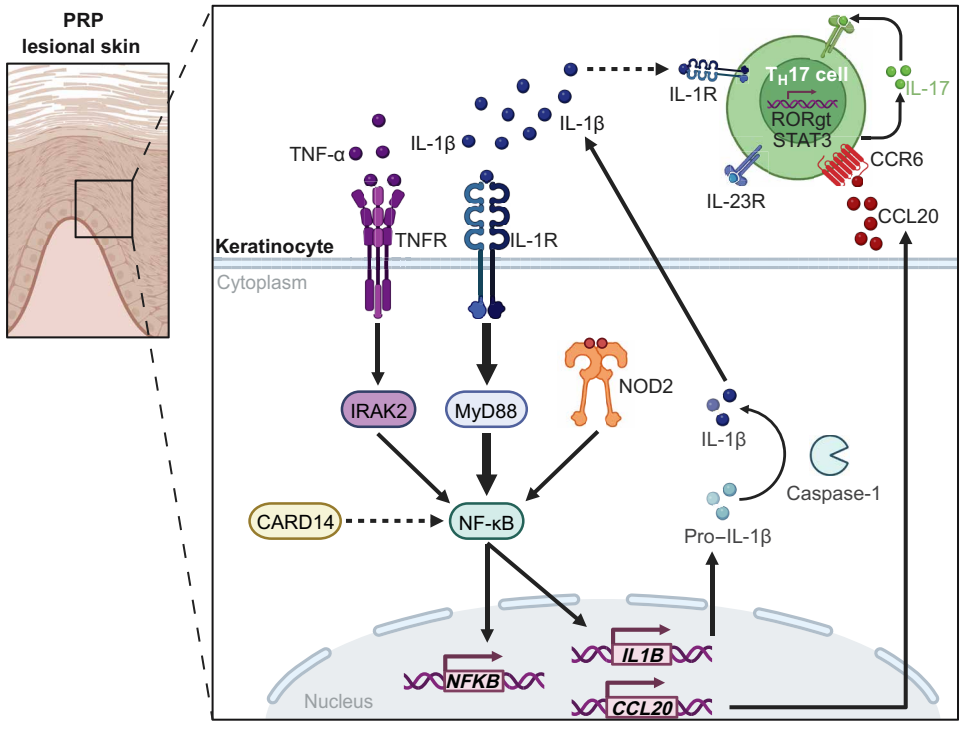

Fig. 6. Proposed pathophysiology of PRP. In keratinocytes, IL-1β signaling through MyD88 activates the NF-κB pathway. Concurrently, activation of this pathway can take place via TNF-α signaling via IRAK2 or directly from NOD2 and CARD14. As a result, there is an up-regulated expression of CCL20, leading to its secretion, and pro–IL-1β, which is potentially cleaved by caspase-1 into its active form, IL-1β, for secretion. The secreted IL-1β binds in a feed-forward loop to its own receptors. The secreted CCL20 attracts T_H17 cells to the keratinocytes through CCR6 binding. IL-1β also can activate T_H17 cells. In this setting, IL-1β would induce not only its own production but also CCL20 production to further attract T_H17 cells, as well as directly activate these T_H17 cells. Created with Biorender.com.

receptor) through its T cell recruitment in the skin, particularly T_H17 cells (*20*–*29*). This is of high interest, as many studies suggest a role of T_H17 cells and their secreted cytokine IL-17 in PRP (*8*, *30*). Moreover, patients responding to anti–IL-17A show a decrease in *CCL20* expression, in contrast to nonresponders, for whom it remains high (*6*, *7*). Our in vitro data show that IL-1β stimulation significantly induces *CCL20* expression in keratinocyte cultures (Fig. 5D) and that IL-1β is the strongest inducer of *CCL20* (Fig. 5F). Therefore, we postulate that the T_H17 cells are involved because of CCL20 recruitment and that the IL-1 axis activation would be the upstream event in this mechanism.

We also hypothesize that the partial responses observed with IL-17 inhibitors could be due to the remaining IL-1β pathway activation, on which IL-17 inhibitors would not have effect. IL-1β would still act upstream of T_H17 cells and activate them via another angle (*31*). IL-1 inhibition would additionally inhibit the homing of T_H17 cells to the skin by abrogating CCL20.

Our data suggests IL-1β expression in keratinocytes of lesional PRP tissue, confirmed by immunofluorescence (Fig. 3H and fig. S5F), which aligns with the strong interaction between IL-1 family genes and keratinocyte function shown by STRING molecular analysis (Fig. 2G), underscoring a keratinocyte-driven inflammation.

We found that UV light increases the production of *CCL20* in human keratinocytes (Fig. 5F and fig. S8F). As UV light activates the inflammasome and IL-1β production via caspase-11 (*32*), this could explain the photosensitivity observed in PRP.

We noticed a rapid clinical improvement within 2 to 3 weeks of IL-1 antagonist therapy in our three patients with PRP, which is faster than usually observed with biologics in other IMIDs such as psoriasis and AD. For instance, psoriasis is understood as an adaptive immunity-driven T_H17-mediated autoimmune disease (*33*). There, the IL-23p19 inhibitor tildrakizumab leads to a PASI50 response in 50% of patients after at least 4 weeks (*34*). In contrast, in innate-driven autoinflammatory diseases such as generalized pustular psoriasis, the IL-36 receptor inhibitor spesolimab clears more than 50% of patients already after 1 week (*35*). This further supports our findings that PRP is driven by an autoinflammatory mechanism and should be classified as an autoinflammatory keratinization disorder.

Of note, Brand *et al.* (*36*) identified transforming growth factor–β (TGF-β) as a stimulant of IL-1β–dependent CCL20 expression in chronic obstructive pulmonary disease. However, in our data in keratinocytes, TGF-β stimulus alone does not increase CCL20 expression (Fig. 5F).

This study faces several limitations, including its retrospective nature and the small patient cohort. A shortage of tissue samples at critical time points, such as weeks 0 and 8, restricted the ability to conduct detailed mechanistic research. Furthermore, the limited scale of our study may not reflect the full diversity seen in complex diseases like PRP. Future research, involving a broader spectrum of patients, is essential to determine the efficacy of targeting IL-1β across the entire PRP patient population. It could also assess whether skin molecular profiling could distinguish between those who would

benefit from such treatments and those who would not. These constraints underscore the urgency of future prospective studies with larger sample sizes to both verify our findings and enhance our understanding of the disease's underlying mechanisms.

Because of the rarity of the disease, the presentation of three patients being treatment refractory is rather selective; therefore, the mechanistic findings were confirmed on a broader patient base across cohorts A and B, which included responders and nonresponders to the respective therapies.

Our study offers a foundational demonstration of a precision medicine strategy guided by molecular insights, affirming the therapeutic potential of targeting the IL-1 pathway, with a specific focus on IL-1β, in the context of PRP. Our data strongly suggest an IL-1–centered regulatory network associated with PRP as further supported by the quick and reproducible improvement in three patients treated with IL-1/IL-1β antagonists. In addition, we propose a mechanism involving NF-κB–mediated IL-1β–CCL20 signaling in PRP, which includes activation of CARD14 and NOD2. Our findings define PRP as an autoinflammatory keratinization disorder, suggesting a novel therapeutic approach. While further clinical studies are essential, our findings support the use of IL-1β antagonists in PRP.

MATERIALS AND METHODS

Experimental design

The objective of the study was to conduct a molecular profiling and transcriptomic analysis of PRP to identify driving pathways and potential targets. Sample size resulted from patient availability. Inclusion required clinical and histological confirmation of PRP diagnosis. Demographical data including medical history and samples from blood and lesional skin [formalin-fixed paraffin-embedded (FFPE) tissues] were collected from 13 patients with a clinically and histologically confirmed diagnosis of PRP type I (adult type) between 2012 and 2015 in the Department of Dermatology, University Hospital Zurich. From eight of those patients, biopsies after resolution of skin disease (post-PRP) were obtained. In addition, FFPE biopsies from psoriasis ($n = 6$), AD ($n = 7$), and HC (anonymized, $n = 8$) were obtained from the biobank of the Department of Dermatology, University Hospital Zurich. Rarely, a biopsy from non-lesional skin in a patient with PRP was performed (cohort A). An external cohort with bulk RNA sequencing (RNA-seq) of patients with PRP [cohort B, derived from Boudreaux *et al.* (*4*)] was used for validation of findings. On the basis of the findings, three treatment-refractory patients were treated with anti–IL-1/anti–IL-1β biologicals and were treated between 2019 and 2023 (cohort C). Because of the retrospective character of the investigation, no predefined prospective measures were applied (e.g., stopping rules for data collection, handling of outliers, endpoints, randomization, and blinding). The study was approved by the local ethics committee (Canton of Zurich), and informed consent was obtained from the patients.

Response was assessed by clinical severity scores [PASI and eczema area and severity index (EASI)], histological measures (acanthosis and papillomatosis index), and IL-1β immunohistochemistry (mean fluorescence intensity). Clinical severity was assessed by EASI in AD and by PASI (*37*) in psoriasis and PRP, as PRP shows the same clinical features as psoriasis (table S1). Severity by PASI is defined as mild < 10, moderate ≥ 10, and severe ≥ 20. Severity grading by EASI is defined as clear = 0, almost clear = 0.1 to 1.0, mild = 1.1 to 7.0, moderate = 7.1 to 21.0, severe = 21.1 to 50.0, and very severe = 50.1 to 72.0 (*38*).

Immunohistochemistry for IL-1β

IL-1β immunohistochemical analysis was conducted on FFPE skin sections obtained from patients. The sections were deparaffinized and subjected to antigen retrieval using sodium citrate buffer. To suppress the activity of endogenous peroxidase in the sections, 3% H_2O_2 was applied. Subsequently, the sections were blocked at room temperature for 60 min using a 5% bovine serum albumin (BSA)/phosphate-buffered saline (PBS) solution. The sections were then incubated overnight at 4°C with goat primary antibodies IL-1β/IL-1F2 (Ala^{117}-Ser^{269}; R&D Systems, catalog no. AF-201-SP; dilution, 1:100) designed not only to detect the mature/cleaved form of IL-1β but also to detect the pro-form and with a mouse pan-cytokeratin (Pan-CK) antibody (C11; Santa Cruz Biotechnology, catalog no. sc-8018; dilution, 1:500). After washing, the sections were incubated for 90 min at room temperature in the dark with secondary antibodies (Invitrogen; Alexa Fluor 488–rabbit anti-goat; dilution, 1:200; and Alexa Fluor 568–donkey anti-mouse; dilution, 1:200) in a 5% BSA/PBS solution. Slides were washed and mounted in ProLong Gold Antifade Mountant with 4′,6-diamidino-2-phenylindole (Therfmo Fisher Scientific). Image intensity measurements were performed using ImageJ software, analyzing three to five fields per skin tissue section. The relative image intensity was calculated as the mean intensity per selected image area.

Immunohistochemistry for CCL20 and caspase-1

Biopsies obtained at baseline (week 0) and week 8 were fixed in formalin and subsequently embedded in paraffin. FFPE tissue sections were heated at 60°C for 30 min, deparaffinized, and rehydrated. Slides were placed in a PH9 antigen retrieval buffer and heated at 125°C for 30 s in a pressure cooker water bath. After cooling, slides were treated with 3% H_2O_2 (5 min) and blocked using 10% goat serum (30 min). Overnight incubation at 4°C was then performed using anti-human primary antibodies anti–caspase-1 (Atlas Antibodies, catalog no. HPA003056) and anti-CCL20 (Sino Biological, catalog no. 10485-T24). Slides were then washed and exposed to secondary antibody, peroxidase (30 min), and diaminobenzidine substrate. Counterstain with hematoxylin and dehydration was done, and slides were mounted and viewed under the microscope.

Sanger sequencing

DNA was extracted from EDTA blood, and primers were designed to cover exons 6 and 7 of the *CARD14* gene. After the initial polymerase chain reaction, the DNA was purified using AMPure Beads (Beckman Coulter), and Sanger sequencing was performed using the Pro Dye Kit (Promega) and then analyzed on a Promega Spectrum Compact instrument (Promega). The generated sequence data were evaluated by using the CLC Software (QIAGEN) and compared to pathogenic variants in exons 6 and 7 of *CARD14* that have been previously associated with PRP.

Targeted RNA-seq (cohort A)

RNA was extracted from FFPE skin biopsies (baseline and week 8) using the RNeasy FFPE kit (QIAGEN GmbH, Hilden, Germany) as per the manufacturer's instructions. RNA quality was checked, and RNA was quantified using a NanoDrop spectrophotometer (NanoDrop Technologies, Oxfordshire, UK). The RNA was then

analyzed with the nCounter Human Immunology panel (Nanostring Technologies, Seattle, USA) following the instructions from the supplier.

Statistical analyses and visualization of data were performed using Rstudio (v4.1.0) and GraphPad Prism (v9.0.0). Differential gene analysis was conducted using the R limma (*39*) package v.3.48.0, and *P* values were from multiple testing corrected using Benjamini and Hochberg (BH) (*40*) false discovery rate (FDR). If not stated otherwise, then all other *P* values were calculated using unpaired two-tailed *t* test. Significant differences were annotated with asterisks: $*P \leq 0.05$, $**P < 0.01$, $***P < 0.001$, and $****P < 0.0001$. For the heatmap, genes were selected on the basis of their contribution to the first three principal components (PC1, PC2, and PC3). For each PC, the 20 genes with the highest positive loadings and the 20 genes with the highest negative loadings (lowest values) were chosen. For correlation analysis, a linear model fit is calculated along with its corresponding *P* value, and *R* values are derived from the Pearson correlation coefficient.

External bulk RNA-seq PRP profile (cohort B) analysis

Data acquisition and DE analysis

The bulk RNA-seq PRP cohort B (Fig. 1A) is derived from Boudreaux *et al.* (*4*). A DE analysis was performed on lesional versus non-lesional tissue, only with samples before treatment. This was carried out with paired samples (by patient id) using DESeq2 (*41*).

Analysis of DE results with IPA

After processing, the DE results were analyzed with the use of QIAGEN IPA (*42*) (QIAGEN Inc., https://digitalinsights.qiagen.com/IPA). In IPA, DE results were filtered, implementing a 0.5 cutoff for absolute LFC and a 0.1 threshold for adjusted *P* value. The IPA software was used to extract the upstream regulators and mechanistic networks. It was also used for enriching ingenuity canonical pathways, annotating diseases or functions, and developing a summary network. The summary network was developed with a minimum setting for the number of nodes. To identify the top activated upstream regulators in PRP, IPA-predicted upstream regulators with an activation *z*-score > 2 were ranked by FDR, and the first five were selected.

Correlation analysis

The whole bulk RNA-seq dataset was processed with DESeq, to normalize the counts using the normTransform function. Subsequently, a total of 1195 genes, which were both highly variable and had high expression levels, were isolated from the dataset. This gene selection was based on criteria where log(mean expression) values were greater than 4 and log(dispersion across samples) exceeded 0.5. Subsequently, a matrix detailing the co-expression correlations was crafted. Hierarchical clustering techniques were adopted to define 10 distinct correlation clusters. Using the scipy library, the correlation matrix was converted into a condensed distance matrix. Hierarchical clustering was then done using the "complete" method, and genes were assigned to 1 of the 10 clusters.

DE and correlation analysis crossover

An overlap was created between the previously run DESEQ2 DE results and the cluster list of genes. A GSEA of the genes in each cluster was run on the DE results.

ORA and PPI network analysis

ORA was run on the list of genes representing each cluster, using GSEApy (*43*) Enrichr module. The genes in cluster 1 were further subjected to a PPI network analysis using STRING (v11.5) (*44*), with default settings. *K*-means analysis, as implemented in STRING (v11.5) (*44*), was used to further subdivide these into eight functionally based subclusters. The ORA was similarly run on the two subclusters of interest.

Treatment transcriptomic response (cohort C)

Data extraction and labeling

Skin biopsies from PRP lesional areas were obtained from two patients before and at week 8 of anakinra treatment, constituting cohort C. The biopsies were processed using the GeoMx Human Whole Transcriptome Atlas. This technique uses mRNA-specific in situ hybridization probes linked to distinct DNA barcodes. Upon selection of a "region of interest" (ROI), these barcodes are detached using UV cleavage. Subsequently, the extracted RNA undergoes sequencing on an Illumina system, generating a transcriptome for each designated ROI. Specific ROIs targeted were the epidermis (Pan-CK) and $CD3^+$ and $CD68^+$ cells. Because of low overall counts in some samples, samples from different selected regions were all pooled together to increase statistical power. This resulted in 24 technical replicates for patient 1 (13 before treatment and 11 during treatment) and 26 for patient 2 (13 before treatment and 13 during treatment). We confirmed that pooling replicates from the different regions together was a reasonable approach as the signal originating from the pooled DE analysis correlated significantly with the signal from the non-pooled analysis (fig. S11). GeoMx Data Analysis Suite was used to extract the raw counts for each replicate in a count matrix, which was further imported to R.

DE analysis

DESEQ2 (*41*) was used for DE analysis of samples from both patients together, comparing pooled replicates during treatment versus before treatment.

Processing of DE results

The results of the DE analysis were analyzed with the use of QIAGEN IPA (*42*) (QIAGEN Inc., https://digitalinsights.qiagen.com/IPA). The DE results were filtered, using the same criteria as mentioned previously: an absolute LFC cutoff of 0.5 and an adjusted *P* value threshold of 0.1. The same extraction and enrichment procedures for upstream regulators, mechanistic networks, ingenuity canonical pathways, disease or function annotations, and summary networks were then performed.

Gene set enrichment analysis

GSEA (*45*) was carried out on the DE results, using GSEApy (*43*) prerank module. In addition, the top positively DEGs in cohort B (*4*) (with an LFC > 0 and adjusted *P* value < 0.05) were selected to form a gene set. This gene set was then used for the GSEA of the DE comparison involving both patients (after versus before treatment).

Naming convention

The treatment signal defines the DE analysis of lesional samples after versus before treatment (in cohort C), and the PRP signature (*PRP*) defines the paired DE of lesional versus non-lesional skin in cohort B (*4*).

In vitro stimulation of keratinocytes

Primary human keratinocytes were stimulated with cytokines (R&D Systems) for 8 hours, and cells were harvested for RNA for RNA-seq. Treatments included unstimulated control, IL-17A (10 ng/ml), interferon (IFN; 5 ng/ml), IFN-α (5 ng/ml), TNF (10 ng/ml), IL-17A and TNF (10 ng/ml for each cytokine), IL-4 (10 ng/ml), IL-13 (10 ng/ml), IL-1β (10 ng/ml), and IL-36γ (10 ng/ml).

DE analysis was performed on the whole transcriptome for 20 controls (non-stimulation) and 20 IL-1β–stimulated samples (paired analysis). GSEA (*45*) analysis was performed on the DE results using the GSEApy (*43*) prerank module for the DEGs in the stimulation. In addition, GSEApy (*43*) Enrichr module was used to perform ORA on genes that were significantly DE with positive LFC in both stimulation and PRP bulk RNA-seq. For *CCL20* expression changes with other stimulations, we ran paired *t* test with scipy.stats.ttest_rel, on the log-normalized count, with FDR correction using the BH method (*40*).

Single-cell dissection of *CARD14* GOF mutation in mice dataset

Processed counts from the *CARD14* GOF mouse model single-cell RNA-seq data (*10*) were obtained from the Gene Expression Omnibus (GEO) accession number GSE204731 in the form of a count matrix. Both samples (control and *CARD14* GOF) were analyzed using Scanpy (*46*) following its base tutorial. Cell types were discerned on the basis of marker gene expression, with keratinocytes and sebocytes chosen for further analysis. The Wilcoxon rank sum test was conducted to evaluate specific expression changes in keratinocytes between the GOF sample and control samples. Subsequently, the GSEApy (*43*) prerank module was used to investigate pathway enrichments associated with the GOF.

Supplementary Materials

This PDF file includes:
Figs. S1 to S11
Legends for tables S1 and S2

Other Supplementary Material for this manuscript includes the following:
Tables S1 and S2

REFERENCES AND NOTES

1. C. Kromer, R. Sabat, D. Celis, R. Mössner, Systemic therapies of pityriasis rubra pilaris: A systematic review. *J. Dtsch. Dermatol. Ges.* **17**, 243–259 (2019).
2. S. Roenneberg, T. Biedermann, Pityriasis rubra pilaris: Algorithms for diagnosis and treatment. *J. Eur. Acad. Dermatol. Venereol.* **32**, 889–898 (2018).
3. D. Haynes, J. L. Strunck, C. A. Topham, A. G. Ortega-Loayza, G. Kent, P. B. Cassidy, R. Hu, K. Choate, Z. Wang, Y. Liu, T. M. Greiling, Evaluation of Ixekizumab treatment for patients with pityriasis rubra pilaris: A single-arm trial. *JAMA Dermatol.* **156**, 668–675 (2020).
4. B. W. Boudreaux, T. P. Pincelli, P. K. Bhullar, M. H. Patel, C. M. Brumfiel, X. Li, M. G. Heckman, M. R. Pittelkow, A. R. Mangold, J. C. Sluzevich, Secukinumab for the treatment of adult-onset pityriasis rubra pilaris: A single-arm clinical trial with transcriptomic analysis. *Br. J. Dermatol.* **187**, 650–658 (2022).
5. H. E. Iredale, S. J. Meggitt, Photosensitive pityriasis rubra pilaris. *Clin. Exp. Dermatol.* **31**, 36–38 (2006).
6. H. Nagai, H. Jimbo, S. Matsuura, S. Tatsuoka, E. Shiraki, C. Nishigori, Successful treatment of pityriasis rubra pilaris with guselkumab: Serum CCL20 as a potential marker for the disease activity. *Dermatol. Ther.* **33**, e14403 (2020).
7. J. L. Strunck, B. Cutler, B. Rajpal, G. Kent, D. Haynes, C. A. Topham, A. G. Ortega-Loayza, D. Yang, Z. Wang, Y. Liu, P. Cassidy, T. M. Greiling, Pityriasis rubra pilaris response to IL-17A inhibition is associated with IL-17C and CCL20 protein levels. *J. Invest. Dermatol.* **142**, 235–239 (2022).
8. D. Haynes, T. Reiter, R. Velasco, M. Chang, R. Kulkarni, G. Kent, J. Strunck, P. Cassidy, T. M. Greiling, Pityriasis rubra pilaris transcriptomics implicate T helper 17 signaling and correlate with response to ixekizumab, with distinct gene expression profiles in nonresponders. *J. Invest. Dermatol.* **143**, 501–504 (2023).
9. D. Fuchs-Telem, O. Sarig, M. A. M. van Steensel, O. Isakov, S. Israeli, J. Nousbeck, K. Richard, V. Winnepenninckx, M. Vernooij, N. Shomron, J. Uitto, P. Fleckman, G. Richard, E. Sprecher, Familial pityriasis rubra pilaris is caused by mutations in CARD14. *Am. J. Hum. Genet.* **91**, 163–170 (2012).
10. T. Yoshikawa, T. Takeichi, T. Hirabayashi, Y. Muro, Y. Miyasaka, T. Ohno, M. Akiyama, IL-17 axis is a significant driver of skin inflammation in Card14 mutant pityriasis rubra pilaris model mice. [Preprint] (2023). https://doi.org/10.21203/rs.3.rs-2513325/v1.
11. J. Bertin, L. Wang, Y. Guo, M. D. Jacobson, J. L. Poyet, S. M. Srinivasula, S. Merriam, P. S. DiStefano, E. S. Alnemri, CARD11 and CARD14 are novel caspase recruitment domain (CARD)/membrane-associated guanylate kinase (MAGUK) family members that interact with BCL10 and activate NF- κB. *J. Biol. Chem.* **276**, 11877–11882 (2001).
12. M. Wang, S. Zhang, G. Zheng, J. Huang, Z. Songyang, X. Zhao, X. Lin, Gain-of-function mutation of *Card14* leads to spontaneous psoriasis-like skin inflammation through enhanced keratinocyte response to IL-17A. *Immunity* **49**, 66–79 (2018).
13. O. Eytan, L. Qiaoli, J. Nousbeck, M. A. M. van Steensel, B. Burger, D. Hohl, A. Taïeb, S. Prey, D. Bachmann, E. Avitan-Hersh, H. J. Chung, A. Shemer, H. Trau, R. Bergman, D. Fuchs-Telem, E. Warshauer, S. Israeli, P. H. Itin, O. Sarig, J. Uitto, E. Sprecher, Increased epidermal expression and absence of mutations in *CARD14* in a series of patients with sporadic pityriasis rubra pilaris. *Br. J. Dermatol.* **170**, 1196–1198 (2014).
14. M. Mellett, B. Meier, D. Mohanan, R. Schairer, P. Cheng, T. K. Satoh, B. Kiefer, C. Ospelt, S. Nobbe, M. Thome, E. Contassot, L. E. French, CARD14 gain-of-function mutation alone is sufficient to drive IL-23/IL-17-mediated psoriasiform skin inflammation in vivo. *J. Invest. Dermatol.* **138**, 2010–2023 (2018).
15. L. Chen, S.-Q. Cao, Z.-M. Lin, S.-J. He, J.-P. Zuo, NOD-like receptors in autoimmune diseases. *Acta Pharmacol. Sin.* **42**, 1742–1756 (2021).
16. W. P. Arend, The balance between IL-1 and IL-1Ra in disease. *Cytokine Growth Factor Rev.* **13**, 323–340 (2002).
17. C. Gabay, C. Lamacchia, G. Palmer, IL-1 pathways in inflammation and human diseases. *Nat. Rev. Rheumatol.* **6**, 232–241 (2010).
18. C. F. Bigler, D. A. Norris, W. L. Weston, W. P. Arend, Interleukin-1 receptor antagonist production by human keratinocytes. *J. Invest. Dermatol.* **98**, 38–44 (1992).
19. D. Gruaz-Chatellard, C. Baumberger, J.-H. Saurat, J.-M. Dayer, Interleukin 1 receptor antagonist in human epidermis and cultured keratinocytes. *FEBS Lett.* **294**, 137–140 (1991).
20. K. Hirota, H. Yoshitomi, M. Hashimoto, S. Maeda, S. Teradaira, N. Sugimoto, T. Yamaguchi, T. Nomura, H. Ito, T. Nakamura, N. Sakaguchi, S. Sakaguchi, Preferential recruitment of CCR6-expressing Th17 cells to inflamed joints via CCL20 in rheumatoid arthritis and its animal model. *J. Exp. Med.* **204**, 2803–2812 (2007).
21. R. Robert, C. Ang, G. Sun, L. Juglair, E. X. Lim, L. J. Mason, N. L. Payne, C. C. A. Bernard, C. R. Mackay, Essential role for CCR6 in certain inflammatory diseases demonstrated using specific antagonist and knockin mice. *JCI Insight* **2**, (2017).
22. L. Zhao, J. Li, B. Jiang, J. Yang, J. Lan, D. Li, J. Wen, Y. Xia, W. Nie, Z. Wang, Y. Lv, F. Zeng, Y. Li, G. Shen, P. Lei, J. Tao, GRP78 downregulation in keratinocytes promotes skin inflammation through the recruitment and activation of CCR6$^+$ IL-17A–Producing γδ T cells. *J. Invest. Dermatol.* 10.1016/j.jid.2023.12.023, (2024).
23. L. Xi, S. Garcet, Z. Ye, K. Hung, M. Hassan-Zahraee, E. Kieras, J. G. Krueger, C. Hyde, E. Peeva, A shared tissue transcriptome signature and pathways in psoriasis and ulcerative colitis. *Sci. Rep.* **12**, 19740 (2022).
24. Z. Shi, X. Wu, C.-Y. Wu, S. P. Singh, T. Law, D. Yamada, M. Huynh, W. Liakos, G. Yang, J. M. Farber, Y.-J. Y. Wan, S. T. Hwang, Bile acids improve psoriasiform dermatitis through inhibition of IL-17A expression and CCL20-CCR6–mediated trafficking of T cells. *J. Invest. Dermatol.* **142**, 1381–1390 (2022).
25. J.-W. Shin, M. Kwon, J. Hwang, S.-J. Lee, J.-H. Lee, H.-J. Kim, K. B. Lee, S.-J. Lee, E. M. Jeong, J. H. Chung, I.-G. Kim, Keratinocyte transglutaminase 2 promotes CCR6$^+$ γδT-cell recruitment by upregulating CCL20 in psoriatic inflammation. *Cell Death Dis.* **11**, 301 (2020).
26. K. Furue, T. Ito, Y. Tanaka, A. Hashimoto-Hachiya, M. Takemura, M. Murata, M. Kido-Nakahara, G. Tsuji, T. Nakahara, M. Furue, The EGFR-ERK/JNK-CCL20 pathway in scratched keratinocytes may underpin Koebnerization in psoriasis patients. *Int. J. Mol. Sci.* **21**, 434 (2020).
27. M. N. Hedrick, A. S. Lonsdorf, A.-K. Shirakawa, C.-C. R. Lee, F. Liao, S. P. Singh, H. H. Zhang, A. Grinberg, P. E. Love, S. T. Hwang, J. M. Farber, CCR6 is required for IL-23–induced psoriasis-like inflammation in mice. *J. Clin. Invest.* **119**, 2317–2329 (2009).
28. T. Mabuchi, T. P. Singh, T. Takekoshi, G. Jia, X. Wu, M. C. Kao, I. Weiss, J. M. Farber, S. T. Hwang, CCR6 is required for epidermal trafficking of γδ-T cells in an IL-23-induced model of psoriasiform dermatitis. *J. Invest. Dermatol.* **133**, 164–171 (2013).
29. K. E. Kim, Y. Houh, H. J. Park, D. Cho, Therapeutic effects of erythroid differentiation regulator 1 on imiquimod-induced psoriasis-like skin inflammation. *Int. J. Mol. Sci.* **17**, 244 (2016).
30. L. Feldmeyer, A. Mylonas, O. Demaria, A. Mennella, N. Yawalkar, E. Laffitte, D. Hohl, M. Gilliet, C. Conrad, Interleukin 23–helper T cell 17 axis as a treatment target for pityriasis rubra pilaris. *JAMA Dermatol.* **153**, 304–308 (2017).
31. S. Revu, J. Wu, M. Henkel, N. Rittenhouse, A. Menk, G. M. Delgoffe, A. C. Poholek, M. J. McGeachy, IL-23 and IL-1β drive human Th17 cell differentiation and metabolic reprogramming in absence of CD28 costimulation. *Cell Rep.* **22**, 2642–2653 (2018).
32. L. Feldmeyer, M. Keller, G. Niklaus, D. Hohl, S. Werner, H.-D. Beer, The inflammasome mediates UVB-induced activation and secretion of interleukin-1β by keratinocytes. *Curr. Biol.* **17**, 1140–1145 (2007).
33. J. Di Domizio, M. Gilliet, Psoriasis caught in the NET. *J. Invest. Dermatol.* **139**, 1426–1429 (2019).

34. A. Blauvelt, H. Sofen, K. Papp, M. Gooderham, S. Tyring, Y. Zhao, S. Lowry, A. Mendelsohn, J. Parno, K. Reich, Tildrakizumab efficacy and impact on quality of life up to 52 weeks in patients with moderate-to-severe psoriasis: A pooled analysis of two randomized controlled trials. *J. Eur. Acad. Dermatol. Venereol.* **33**, 2305–2312 (2019).
35. H. Bachelez, S.-E. Choon, S. Marrakchi, A. D. Burden, T.-F. Tsai, A. Morita, A. A. Navarini, M. Zheng, J. Xu, H. Turki, M. J. Anadkat, S. Rajeswari, H. Hua, S. D. Vulcu, D. Hall, K. Tetzlaff, C. Thoma, M. G. Lebwohl, Trial of spesolimab for generalized pustular psoriasis. *N. Engl. J. Med.* **385**, 2431–2440 (2021).
36. O. J. Brand, S. Somanath, C. Moermans, H. Yanagisawa, M. Hashimoto, S. Cambier, J. Markovics, A. J. Bondesson, A. Hill, D. Jablons, P. Wolters, J. Lou, J. D. Marks, J. L. Baron, S. L. Nishimura, Transforming growth factor-β and interleukin-1β signaling pathways converge on the chemokine CCL20 promoter. *J. Biol. Chem.* **290**, 14717–14728 (2015).
37. T. Fredriksson, U. Pettersson, Severe psoriasis–oral therapy with a new retinoid. *Dermatologica* **157**, 238–244 (1978).
38. Y. A. Leshem, T. Hajar, J. M. Hanifin, E. L. Simpson, What the Eczema Area and Severity Index score tells us about the severity of atopic dermatitis: An interpretability study. *Br. J. Dermatol.* **172**, 1353–1357 (2015).
39. M. E. Ritchie, B. Phipson, D. Wu, Y. Hu, C. W. Law, W. Shi, G. K. Smyth, *limma* powers differential expression analyses for RNA-sequencing and microarray studies. *Nucleic Acids Res.* **43**, e47 (2015).
40. Y. Benjamini, Y. Hochberg, Controlling the false discovery rate: A practical and powerful approach to multiple testing. *J. R. Stat. Soc. B. Methodol.* **57**, 289–300 (1995).
41. M. I. Love, W. Huber, S. Anders, Moderated estimation of fold change and dispersion for RNA-seq data with DESeq2. *Genome Biol.* **15**, 550 (2014).
42. A. Krämer, J. Green, J. Pollard Jr., S. Tugendreich, Causal analysis approaches in ingenuity pathway analysis. *Bioinformatics* **30**, 523–530 (2014).
43. Z. Fang, X. Liu, G. Peltz, GSEApy: A comprehensive package for performing gene set enrichment analysis in Python. *Bioinformatics* **39**, btac757 (2023).
44. D. Szklarczyk, A. L. Gable, D. Lyon, A. Junge, S. Wyder, J. Huerta-Cepas, M. Simonovic, N. T. Doncheva, J. H. Morris, P. Bork, L. J. Jensen, C. von Mering, STRING v11: Protein-protein association networks with increased coverage, supporting functional discovery in genome-wide experimental datasets. *Nucleic Acids Res.* **47**, D607–D613 (2019).
45. A. Subramanian, P. Tamayo, V. K. Mootha, S. Mukherjee, B. L. Ebert, M. A. Gillette, A. Paulovich, S. L. Pomeroy, T. R. Golub, E. S. Lander, J. P. Mesirov, Gene set enrichment analysis: A knowledge-based approach for interpreting genome-wide expression profiles. *Proc. Natl. Acad. Sci. U.S.A.* **102**, 15545–15550 (2005).
46. F. A. Wolf, P. Angerer, F. J. Theis, SCANPY: Large-scale single-cell gene expression data analysis. *Genome Biol.* **19**, 15 (2018).

Acknowledgments: We acknowledge H.-D. Beer, A. Duda, M. Nikolaou, D. Hug, J. Käsler, F. Sella, and T. Dittmar for support of this study. We acknowledge the editing support from Life Science Editors. We thank P. Purcell for help with proofreading and editing. **Funding:** This work was supported by the Discovery Grant from the National Psoriasis Foundation (to A.G.A.K.) and University of Zurich (to A.G.A.K.); Orion Research Foundation (to E.S); Yrjö Jahnsson Foundation (to E.S); Vilho, Yrjö and Väisälä Fund (to E.S); Aarne Koskelon foundation (to E.S); Antti and Tyyne Soininen Foundation (to E.S.); and SwissLife Jubiläumsstiftung (to E.C). **Author contributions:** Conceptualization: E.S., Y.S., E.C., and A.G.A.K. Methodology: E.S., Y.S., E.C., and A.G.A.K. Investigation: E.S., Y.S., A.M., S.N., L.C.T., J.N., A.S., E.C., and A.G.A.K. Visualization: E.S., Y.S., E.C., and A.G.A.K. Funding acquisition: E.S., S.L.-K., M.U.K., B.S., M.K., J.E.G., G.C.T., E.C., and A.G.A.K. Project administration: E.S., Y.S., E.C., and A.G.A.K. Mentorship: S.L.-K., M.U.K., B.S., M.K., J.E.G., and G.C.T. Supervision: A.G.A.K. Writing—original draft: E.S., Y.S., E.C., and A.G.A.K. Writing—review and editing: all authors. **Competing interests:** A.M. has no relevant disclosures. He has consulted for Kyowa, Eli Lilly, Momenta, UCB, and Regeneron in the past, greater than 24 months ago. He has consulted for PHELEC in the past, greater than 12 months ago. He has consulted for Incyte, Soligenix, Clarivate, and Bristol Myers Squibb in the past, less than 12 months ago. He consults for Nuvig, Argenyx, Boehringer, Janssen, and Ingelheim now. He consults for Regeneron and Pfizer now with payments to the institution. He has grant support from Kyowa, Miragen, Regeneron, Corbus, Pfizer, Incyte, Eli Lilly, Aregenx, Palvella, Abbvie, Priovant, Merck in the past 24 months. Beyond 24 months, grant support has come from Sun Pharma, Elorac, Novartis, and Janssen. His current patents include Methods and Materials for assessing and treating cutaneous squamous cell carcinoma (provisional 63-423254), use of oral JAKi in Lichen Planus (provisional 63/453,065), and Topical Ruxolitinib in Lichen Planus (WO2022072814A1). The other authors declare that they have no competing interests. **Data and materials availability:** All data needed to evaluate the conclusions in the paper are present in the paper and/or the Supplementary Materials. Cohort A and B data can be found on GEO (A: GSE264192; and B: GSE262954). Other data can be found on Zenodo (cohort C: 10.5281/zenodo.11002999; transcriptional response of keratinocyte to IL1B stimulation: https://doi.org/10.5281/zenodo.10966907; and CCL20 expression in Keratinocytes in response to different stimuli: https://doi.org/10.5281/zenodo.10971502).

Submitted 23 January 2024
Accepted 29 May 2024
Published 3 July 2024
10.1126/sciadv.ado2365